Quantum Phase Transition of Correlated Iron-Based Superconductivity in $LiFe_{1-x}Co_xAs$

Jia-Xin Yin,[1,*,†] Songtian S. Zhang,[1,*] Guangyang Dai,[2,*] Yuanyuan Zhao,[3,*] Andreas Kreisel,[4,*] Gennevieve Macam,[5,*] Xianxin Wu,[2,14] Hu Miao,[6] Zhi-Quan Huang,[5] Johannes H. J. Martiny,[7] Brian M. Andersen,[8] Nana Shumiya,[1] Daniel Multer,[1] Maksim Litskevich,[1] Zijia Cheng,[1] Xian Yang,[1] Tyler A. Cochran,[1] Guoqing Chang,[1] Ilya Belopolski,[1] Lingyi Xing,[2] Xiancheng Wang,[2] Yi Gao,[9] Feng-Chuan Chuang,[5] Hsin Lin,[10] Ziqiang Wang,[11] Changqing Jin,[2] Yunkyu Bang,[12] and M. Zahid Hasan[1,13,‡]

[1]*Laboratory for Topological Quantum Matter and Advanced Spectroscopy (B7), Department of Physics, Princeton University, Princeton, New Jersey 08544, USA*

[2]*Institute of Physics, Chinese Academy of Sciences, Beijing 100190, China*

[3]*School of Physics and Optoelectronic Engineering, Nanjing University of Information Science and Technology, Nanjing 210044, China*

[4]*Institut für Theoretische Physik, Universität Leipzig, D-04103 Leipzig, Germany*

[5]*Department of Physics, National Sun Yat-Sen University, Kaohsiung 80424, Taiwan*

[6]*Condensed Matter Physics and Materials Science Department, Brookhaven National Laboratory, Upton, New York 11973, USA*

[7]*Center for Nanostructured Graphene (CNG), Department of Physics, Technical University of Denmark, DK-2800 Kongens Lyngby, Denmark*

[8]*Niels Bohr Institute, University of Copenhagen, Universitetsparken 5, DK-2100 Copenhagen Ø, Denmark*

[9]*Center for Quantum Transport and Thermal Energy Science, Jiangsu Key Lab on Opto-Electronic Technology, School of Physics and Technology, Nanjing Normal University, Nanjing 210097, China*

[10]*Institute of Physics, Academia Sinica, Taipei 11529, Taiwan*

[11]*Department of Physics, Boston College, Chestnut Hill, Massachusetts 02467, USA*

[12]*Asia Pacific Center for Theoretical Physics and Department of Physics, POSTECH, Pohang, Gyeongbuk, 790-784, Korea*

[13]*Materials Sciences Division, Lawrence Berkeley National Laboratory, Berkeley, California 94720, USA*

[14]*Institut für Theoretische Physik und Astrophysik, Julius-Maximilians-Universität Würzburg, 97074 Würzburg, Germany*

(Received 16 August 2019; published 20 November 2019)

The interplay between unconventional Cooper pairing and quantum states associated with atomic scale defects is a frontier of research with many open questions. So far, only a few of the high-temperature superconductors allow this intricate physics to be studied in a widely tunable way. We use scanning tunneling microscopy to image the electronic impact of Co atoms on the ground state of the $LiFe_{1-x}Co_xAs$ system. We observe that impurities progressively suppress the global superconducting gap and introduce low energy states near the gap edge, with the superconductivity remaining in the strong-coupling limit. Unexpectedly, the fully opened gap evolves into a nodal state before the Cooper pair coherence is fully destroyed. Our systematic theoretical analysis shows that these new observations can be quantitatively understood by the nonmagnetic Born-limit scattering effect in an $s\pm$-wave superconductor, unveiling the driving force of the superconductor to metal quantum phase transition.

DOI: 10.1103/PhysRevLett.123.217004

In the research of high-T_c superconductors, chemical substitution is a powerful way to manipulate electronic phases [1–5]. Meanwhile, chemical substitution also creates imperfections at the atomic scale, which break the unconventional Cooper pairing [4,5]. Although the single atomic impurity pair-breaking effect has been demonstrated in certain superconducting systems [4,5], it is challenging to study its collective many-body manifestation (the finite-density-impurity problem) in a widely tunable way, due to the existence of competing orders or inhomogeneity from strong electron correlation [1–5]. In this regard, $LiFe_{1-x}Co_xAs$ is a rare case in which Co substitution monotonically suppresses the homogeneous superconductivity in LiFeAs without generating other competing orders [6–12], making it a versatile platform to quantitatively test many-body theories. Intriguingly, photoemission, optical, and magnetic response experiments [7–12] reveal that Co substitution changes the Fermi surface and enhances the Fermi surface nesting along with the associated low-energy spin fluctuation, while the spin fluctuation is generally believed to be beneficial for the Cooper pairing in this material [13–15]. This contrast implies a striking, yet not understood depairing mechanism associated with Co substitution. Unexpectedly, previous STM experiments found no detectable local pair-breaking effects associated with a single Co impurity [16,17]. There is also no direct spectroscopic data measured

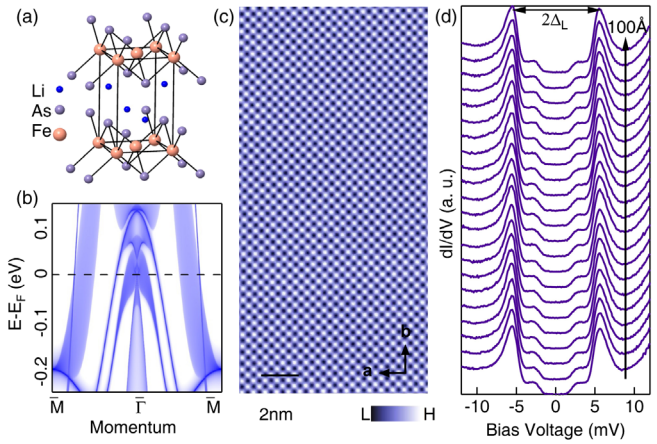

FIG. 1. (a) Crystal structure of LiFeAs. (b) First-principles calculation of the band structure for the (001) surface. (c) Atomically resolved topographic image of pristine LiFeAs showing clean tetragonal lattice. (d) Line-cut differential conductance spectra on pristine LiFeAs, showing a spatially homogeneous double-gap structure.

deep in the superconducting state, demonstrating how a finite density of Co impurities collectively suppresses Cooper pairing. Therefore, a systematic microscopic examination of the effect of the Co substitution on the ground state of $LiFe_{1-x}Co_xAs$ across the whole superconducting phase diagram is demanded.

LiFeAs crystallizes in a tetragonal unit cell ($P4/nmm$) as shown in Fig. 1(a) with a superconducting transition temperature T_c of ~17 K. In momentum space, it features holelike Fermi surfaces at the Brillouin zone center and electronlike Fermi surfaces around the zone boundary, with two extra Dirac cones at the zone center being recently observed [12] [Fig. 1(b)]. We first probe the superconducting ground state of the pristine material at $T = 0.4$ K. Our atomically resolved high resolution STM image reveals a tetragonal lattice which is the Li-terminating surface [Fig. 1(c)]. A line cut of the differential conductance spectra probing the local density of states (DOS) shows a spatially homogenous double-gap structure, with a larger gap of 6.0 meV and a smaller gap of 3.3 meV [Fig. 1(d)]. Based on previous photoemission data [18] measured at 8 K, the large gap likely arises from the electron bands and the inner holelike band, and the smaller gap likely arises from the outer holelike band.

As the Fe lattice is systematically substituted with Co atoms, the T_c decreases linearly and reaches zero around $x = 16\%$ [Fig. 2(a)] [6–11]. Based on the photoemission data [12], the Fermi level can be systematically tuned by increasing Co concentration as illustrated in the inset of Fig. 2(a). Upon bulk substitution of 1% Co atoms, STM topographical scans reveal new dumbbell-like defects randomly scattered on the surface [Fig. 2(b)] that are different from various native defects in LiFeAs. The concentration of these defects is consistent with the nominal Co substitution. The dumbbell-like defects are also randomly aligned along two orthogonal directions, with its local twofold symmetry arising from the structural geometry. The center of each such defect is located at the middle of two Li atoms [Fig. 2(c)], which corresponds to the position of the Co atom in the underlying (Fe, Co) lattice [Fig. 2(d) inset], and altogether they possess a local twofold symmetry. Thus, these defects are likely caused by the atomic Co substitution [17]. Directly above these dumbbell defects, we observe a state near the smaller gap at the positive energy while the overall gap structure remains almost unchanged compared with the far away spectrum [Fig. 2(d)]. The weak in-gap state is consistent with earlier calculations [19] based on the band structure and impurity potentials of Co obtained from density functional theory. We note that the observation of the small local electronic variation may benefit from our lower temperature (0.4 K) and more dilute impurity concentration compared with previous STM studies [16,17]. Our observation indicates that the dilute Co substitution has a limited local impact on the superconducting order parameter or causes only very weak pair-breaking scattering.

With increasing Co concentration, the Co induced weak in-gap states overlap spatially, making them difficult to be visualized individually [16,17]. On the other hand, the finite concentration of Co impurities collectively suppresses bulk superconductivity. To study the global effects on the superconducting ground state, we systematically probe the spectra away from the apparent surface defects for a wide range of Co concentrations at base temperature 0.4 K. We observe a strong variation of the superconducting gap structure in the tunneling conductance which correlates strongly with the T_c reduction [Fig. 2(e)]. As the Co concentration increases, the large superconducting gap size decreases progressively until no gap remains at $x = 16\%$, where $T_C = 0$. Meanwhile, the superconducting coherence peak grows progressively weaker. Evidently, the spectral bottom evolves from a U shape to a V shape and then gradually elevates to the normal state value.

The Co induced gap reduction and scattering can also be qualitatively reflected in the vortex excitation. We extensively study the vortices (Fig. 3) for different Co concentrations at 0.4 K with c-axis magnetic fields. In the pristine sample [Fig. 3(a)], the vortices form an ordered hexagonal lattice under a zero-field cooling method [20,21], as can be clearly seen in the autocorrelation of the real-space mapping at 2 T [Fig. 3(a) inset]. As the Co concentration x increases, we find the vortex lattice symmetry to remain hexagonal-like [Fig. 3(b) inset], while the vortex core size increases. The persistent hexagonal vortex lattice symmetry indicates that the randomly distributed Co dopants do not distort the vortex lattice significantly. As the core size is related with the coherence length which is proportional to the reverse of the gap in the BCS theory, the increment of the vortex core size is consistent with the aforementioned gap reduction. Moreover, measuring the conductance within

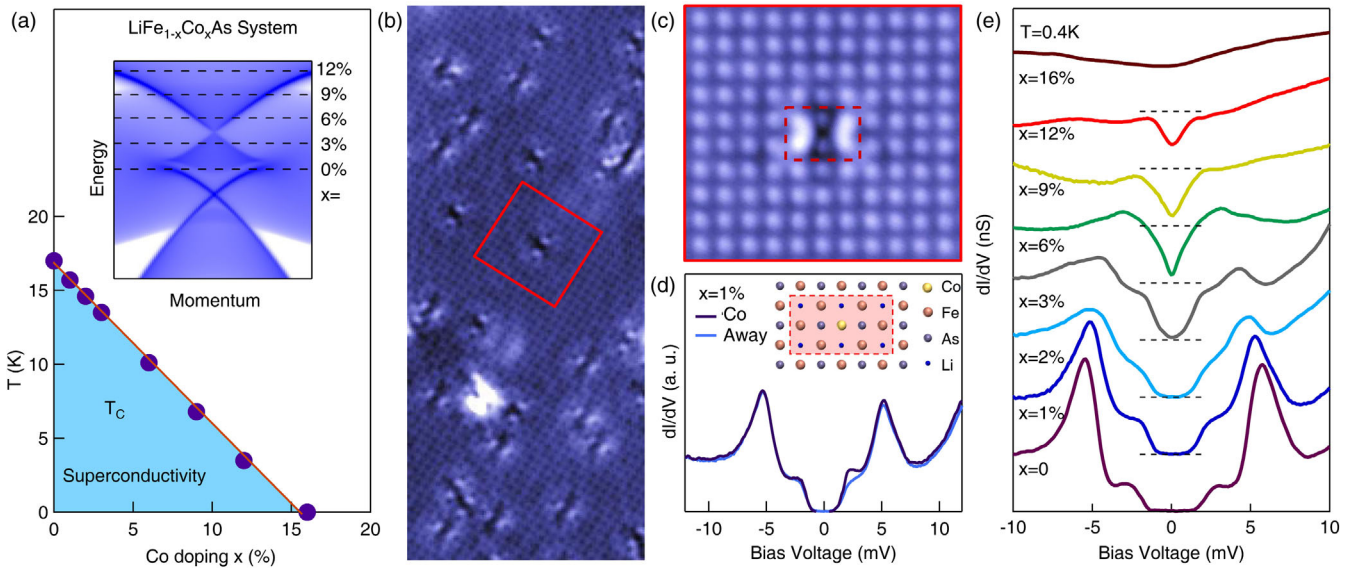

FIG. 2. (a) Phase diagram of $LiFe_{1-x}Co_xAs$. The superconducting transition temperature is determined by the onset of zero resistivity. Inset: illustration of the Co doping effect on the bulk Dirac cone at the Brillouin zone center based on Ref. [12]. (b) Atomically resolved topographic image of a sample with 1% Co substitution, showing randomly scattered dumbbell-like defects that do not exist in the pristine sample and with concentration consistent with the Co substitution level. (c) Enlarged image of single reproducible dumbbell-like defect. The center of the defect geometrically corresponds to a Co substitution atom in the Fe layer [in reference to Fig. 2(d) inset]. (d) Differential conductance spectrum taken at the defect and far from the defect. Inset: crystal structure from top view. (e) Co concentration dependence on spatially averaged superconducting gap structure. The spectra are offset for clarity. The dashed lines mark the zero-intensity value for each case. 30 to 50 dI/dV curves taken away from apparent surface impurities with the same junction setup ($V = -15$ mV, $I = 750$ pA) were averaged to obtain the dI/dV curve for each concentration.

a vortex under an applied c-axis field of 0.5 T reveals sharp in-gap bound states at $|E| \approx 1$ meV [Fig. 3(b)] [20,21], in agreement with the estimate of vortex core state energies in the quantum limit, which should be on the order of a nontopological superconducting vortex state (in the energy order of $\pm\Delta^2/E_F$). As the doping concentration increases, these sharp bound states become gradually less pronounced [Fig. 3(b)], consistent with the aforementioned increased scattering. For each concentration, we carefully examine at least six vortex core states, but do not find any that exhibits a pronounced zero-energy peak. This absence of localized zero-energy states is consistent with the detailed band topology of $LiFe_{1-x}Co_xAs$. According to the photoemission study [12] and first-principles calculations [Figs. 1(b) and 2(a), inset], the surface Dirac cone (lower cone) is buried below the Fermi level in the three-dimensional bulk states, and hence does not form surface helical Cooper pairing and distinct Majorana bound states localized at the ends of the vortex line [22]. Moreover, the expected spectra of the vortex lines in superconductors with bulk Dirac states are not yet fully understood. Recently, there have been theoretical studies of the expected Majorana modes [23,24]. However, details of

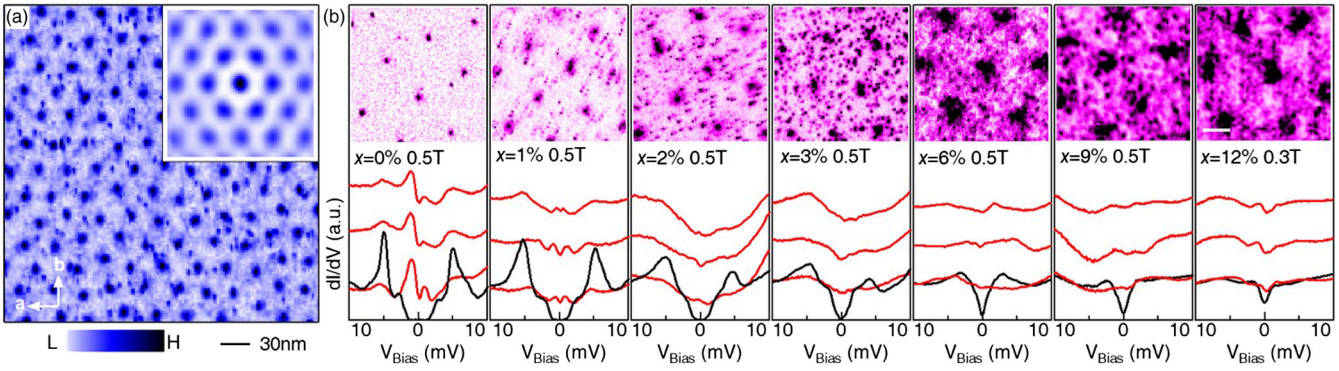

FIG. 3. (a) Left: real space mapping of vortices at the Fermi energy on pristine LiFeAs at $B = 2$ T. Inset: auto-correlation of vortex mapping showing hexagonal lattice symmetry. (b) Spectra in the zero-field state (black) and at three representative vortices offset for clarity (red) for each concentration. The inset image in each panel shows the respective vortex lattice (the bar marks a length of 35 nm).

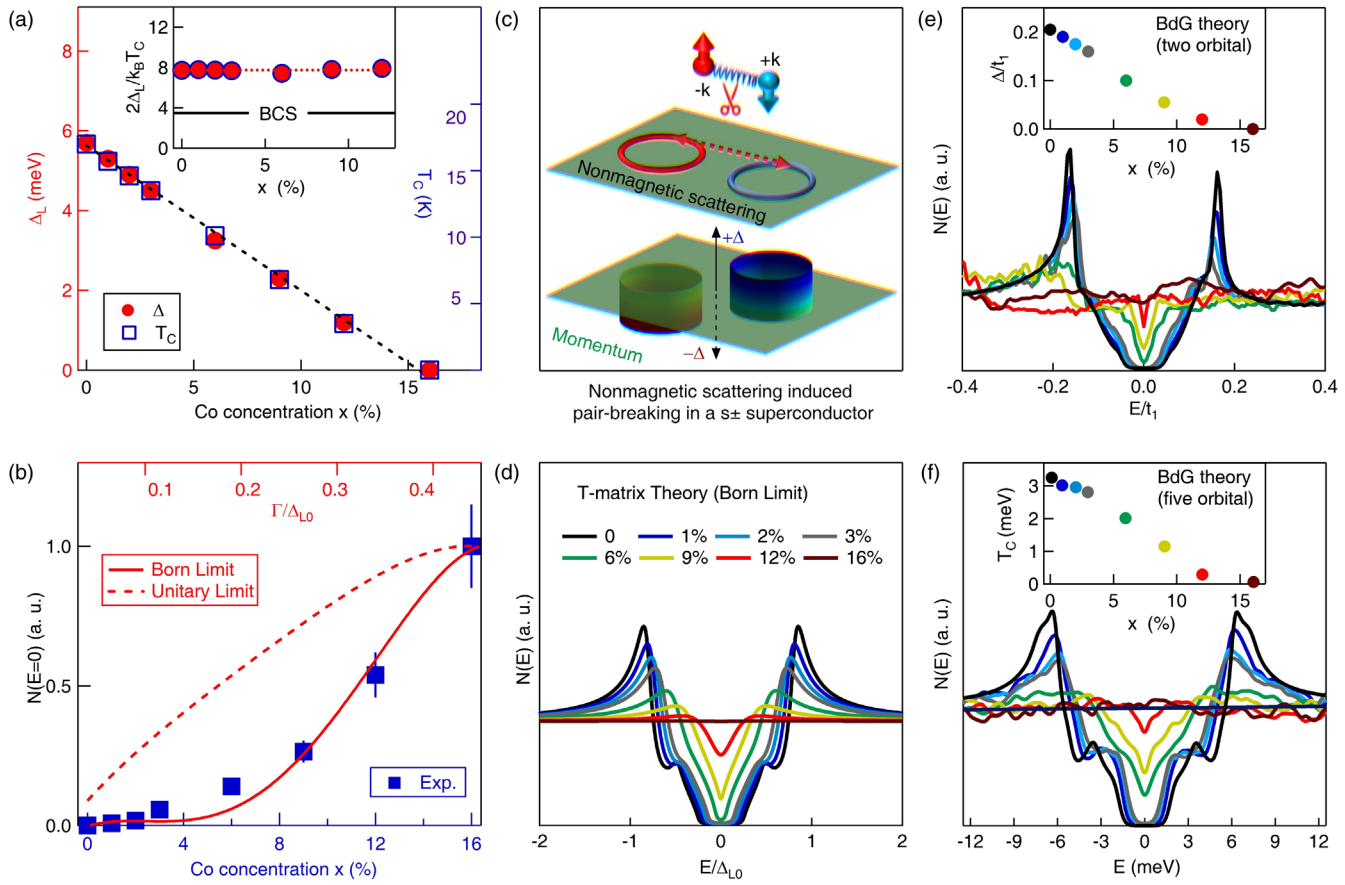

FIG. 4. (a) The large gap size Δ_L (left axis, red) and T_c (right axis, blue) both decrease linearly as a function of concentration x. Inset: $2\Delta_L/k_BT_C$ remains constant (~7.7) as a function of Co concentration. (b) Differential conductance at zero energy $N(E=0)$ as a function of Co concentration x in $LiFe_{1-x}Co_xAs$. The experimental data are normalized by the normal state value. The red solid and dashed lines denote $N(E=0)$ calculated based on Born and unitary limit scattering, respectively. (c) Schematic showing a sign reversal s-wave pairing on two Fermi surfaces (lower panel, $s\pm$-gap symmetry) and the nonmagnetic impurities induced interband scattering causing pair-breaking (upper panel). (d) Calculated density of states evolution of the $s\pm$-pairing state with nonmagnetic scattering at the Born limit with T-matrix theory. (e) (f) Calculated averaged DOS evolution with increasing Co concentration by BdG theory with two-orbital and five-orbital models, respectively. The inset shows the phase diagram plot.

the vortex properties leave the possibility that these states are not localized at the vortex ends and the system might not feature zero energy bound states. These conclusions are not inconsistent with our experimental data, and we want to stress that it is a challenge to unambiguously distinguish the non-localized Majorana state by STM techniques alone [23,24].

To quantify the Co induced gap reduction and scattering, we extract two key parameters from the raw data: the large energy gap size Δ_L and global zero-energy density of state $N(E=0)$. Remarkably, we find that Δ_L decreases linearly as a function of x and reaches zero around 16%, which scales linearly with the reducing T_c [Fig. 4(a)]. In other words, the coupling strength $2\Delta_L/k_BT_C$ remains a constant [inset of Fig. 4(a)]. In particular, $LiFe_{1-x}Co_xAs$ remains in the strong coupling limit for all x as evidenced by $2\Delta_L/k_BT_C \approx 7.7$, much larger than the BCS value 3.5. These results suggest that the superconductivity is destroyed via a mechanism which decreases the pair susceptibility strength, but not the coupling strength. On the other hand, the extracted zero-energy state $N(E=0)$ exhibits an exponential-like growth as shown in Fig. 4(b). The comparatively smaller rate of growth increase of $N(E=0)$ at low concentrations is consistent with the local effect of each Co atom individually [Fig. 2(d)] that each Co induces weak impurity state near the superconducting gap edge [Fig. 2(d)]. As the concentration increases, the interference of their impurity wave functions becomes stronger and the global impurity states spread further in energy, and their tail states eventually contribute to the rapid rise of the global zero-energy state.

In our systematic first-principles calculations, we find that the Co dopants are essentially nonmagnetic with a relatively weak on-site potential of −0.43 eV (Supplemental Material [25]), consistent with previous studies showing that they do not introduce a local magnetic moment [6,10,11,25]. According to the Anderson theorem, nonmagnetic impurities have little effect on the conventional s-wave superconductor. With a sign change in the order, a nonmagnetic impurity is

then able to break the Cooper pairs [4,5,45–48]. Considering previous phase sensitive experiments [21] in this compound, the strongest pairing wave-function candidate is $s\pm$ (where the sign changes between the ordinary hole and electron Fermi surfaces). Crucially, the variation of the gap structure from U shape to V shape due to nonmagnetic scattering in the $s\pm$ pairing state has been predicted using the T-matrix theory [45]. Taking this two-band model from Ref. [45], we set both linear gap reduction and linear scattering rate enhancement with increasing x (Supplemental Material [25]), and compute $N(E=0)$ under the Born (weak scattering) limit and the unitary (strong scattering) limit [4,5] with the results shown in Fig. 4(b). We find that the experimental data are consistent with the former condition and deviates substantially from the latter. Figure 4(d) displays the calculated DOS in the Born limit, which gradually evolves from a fully opened gap to a less coherent V-shaped structure, in consistency with our experimental observation [Fig. 2(e)]. In this model, such behavior is due to the impurity states residing near the gap edge (which can be qualitatively identified from the imaginary part of the quantum many-body self-energy, as detailed in the Supplemental Material [25]) with their tail states gradually moving towards zero energy. Therefore, this theory offers a heuristic understanding of our experiment, demonstrating the Born limit nonmagnetic scattering nature of Co and sign reversal of the gap symmetry.

To acquire a self-consistent and quantitative understanding of the quantum many-body effect of the Co dopants, we further perform real-space calculations using the Bogoliubov–de Gennes (BdG) approach. We first take a two-orbital effective model capturing the essence of its low energy multiband structure and consider randomly distributed electron dopants with weak potential scattering as Co impurities in reference to first-principles calculation (Supplemental Material [25]). The next-nearest-neighbor intra-orbital attraction is considered to cause the $s\pm$-wave Cooper pairing. The calculated DOS indeed shows a clear U-shape to a V-shape evolution as demonstrated in Fig. 4(f). This encourages us to further perform a fully realistic calculation with complete five orbitals. The five-orbital model has successfully explained the vortex core states [20] and weak Co impurity states in pristine LiFeAs [16,19,48], where the $s\pm$-wave Cooper pairing is self-consistently obtained within spin-fluctuation mediated pairing. Considering similarly weak potential scattering, the calculated DOS and phase diagram are shown in Fig. 4(e), which reasonably agrees with the experiment in realistic energy units. We stress that the latter five-band theoretical study contains no free-fitting parameters since the band, gap structure, and impurity potential are fixed by either experiment or first-principles calculations. In this respect, it constitutes a new level of quantitative disorder modeling of unconventional superconductors. Therefore, these realistic self-consistent calculations capture the essence of the experiments and embrace the same spirit of the T-matrix calculation, unambiguously demonstrating the scattering nature of Co in iron-based superconductivity.

Our systematic experimental-theoretical analysis of the impurity effect from a single impurity to the finite density case microscopically uncovers that the Born-limit nonmagnetic scattering is the driving force of the superconducting quantum phase transition in $LiFe_{1-x}Co_xAs$. Future characterization of the impurity effect by Bogoliubov quasiparticle interference imaging and vector field perturbations [21,49] will be important for further exploring the orbital and band selectivity of the Born-limit nonmagnetic scattering.

Experimental and theoretical work at Princeton University was supported by the Gordon and Betty Moore Foundation (GBMF4547/ Hasan) and the United States Department of energy (US DOE) under the Basic Energy Sciences programme (Grant No. DOE/BES DE-FG-02-05ER46200). M. Z. H. acknowledges support from Lawrence Berkeley National Laboratory and the Miller Institute of Basic Research in Science at the University of California, Berkeley in the form of a Visiting Miller Professorship. This work benefited from partial lab infrastructure support under NSF-DMR-1507585. M. Z. H. also acknowledges visiting scientist support from IQIM at the California Institute of Technology. C. J. is supported by NSF & MOST of China through research projects. Y. Z. is supported by the National Natural Science Foundation of China (Grant No. 11804163) and the Natural Science Foundation of the JiangSu Higher Education Institutions of China (Grant No. 18KJB140006). F. C. C. acknowledges support from the National Center for Theoretical Sciences and the Ministry of Science and Technology of Taiwan under Grant No. MOST-107-2628-M-110-001-MY3. He is also grateful to the National Center for High-performance Computing for computer time and facilities. We also acknowledge Korea NRF (Grant No. 2016-R1A2B4-008758), the Natural Science Foundation from Jiangsu Province of China (Grant No. BK20160094). Computations for this work were partially done with resources of Leipzig University Computing Centre. Z. W and K. J. acknowledge US DOE Grant No. DE-FG02-99ER45747. J. H. J. M. is supported by the Danish National Research Foundation, Project DNRF103. B. M. A. acknowledges support from the Independent Research Fund Denmark Grant No. DFF-6108-00096.

*These authors contributed equally to this work.
†Corresponding author.
jiaxiny@princeton.edu
‡Corresponding author.
mzhasan@princeton.edu;

[1] B. Keimer and J. E. Moore, The physics of quantum materials, Nat. Phys. **13**, 1045 (2017).
[2] E. Fradkin, S. A. Kivelson, and J. M. Tranquada, Colloquium: Theory of intertwined orders in high temperature superconductors, Rev. Mod. Phys. **87**, 457 (2015).

[3] G. R. Stewart, Superconductivity in iron compounds, Rev. Mod. Phys. **83**, 1589 (2011).
[4] A. V. Balatsky, I. Vekhter, and J.-X. Zhu, Impurity-induced states in conventional and unconventional superconductors, Rev. Mod. Phys. **78**, 373 (2006).
[5] H. Alloul, J. Bobroff, M. Gabay, and P. J. Hirschfeld, Defects in correlated metals and superconductors, Rev. Mod. Phys. **81**, 45 (2009).
[6] M. J. Pitcher *et al.*, Compositional control of the superconducting properties of LiFeAs, J. Am. Chem. Soc. **132**, 10467 (2010).
[7] S. V. Borisenko *et al.*, Superconductivity without Nesting in LiFeAs, Phys. Rev. Lett. **105**, 067002 (2010).
[8] S. Aswartham *et al.*, Suppressed superconductivity in charge-doped $Li(Fe_{1-x}Co_x)As$ single crystals, Phys. Rev. B **84**, 054534 (2011).
[9] Z. R. Ye *et al.*, Extraordinary Doping Effects on Quasiparticle Scattering and Bandwidth in Iron-Based Superconductors, Phys. Rev. X **4**, 031041 (2014).
[10] Y. M. Dai *et al.*, Spin-Fluctuation-Induced Non-Fermi-Liquid Behavior with Suppressed Superconductivity in $Li(Fe_{1-x}Co_x)As$, Phys. Rev. X **5**, 031035 (2015).
[11] Yu Li *et al.*, Orbital Selective Spin Excitations and their Impact on Superconductivity of $LiFe_{1-x}Co_xAs$, Phys. Rev. Lett. **116**, 247001 (2016).
[12] P. Zhang *et al.*, Multiple topological states in iron-based superconductors, Nat. Phys. **15**, 41 (2019).
[13] A. E. Taylor, M. J. Pitcher, R. A. Ewings, T. G. Perring, S. J. Clarke, and A. T. Boothroyd, Antiferromagnetic spin fluctuations in LiFeAs observed by neutron scattering. Phys. Rev. B **83**, 220514 (2011).
[14] M. P. Allan *et al.*, Identifying the 'fingerprint' of antiferromagnetic spin fluctuations in iron pnictide superconductors, Nat. Phys. **11**, 177 (2015).
[15] P. J. Hirschfeld, M. M. Korshunov, and I. I. Mazin, Gap symmetry and structure of Fe-based superconductors, Rep. Prog. Phys. **74**, 124508 (2011).
[16] S. Chi *et al.*, Impact of iron-site defects on superconductivity in LiFeAs, Phys. Rev. B **94**, 134515 (2016).
[17] H. Yang, Z. Wang, D. Fang, S. Li, T. Kariyado, G. Chen, M. Ogata, T. Das, A. V. Balatsky, and H.-H. Wen, Unexpected weak spatial variation in the local density of states induced by individual Co impurity atoms in superconducting $Na(Fe_{1-x}Co_x)As$ crystals revealed by scanning tunneling spectroscopy, Phys. Rev. B **86**, 214512 (2012).
[18] K. Umezawa *et al.*, Unconventional Anisotropic s-Wave Superconducting Gaps of the LiFeAs Iron-Pnictide Superconductor, Phys. Rev. Lett. **108**, 037002 (2012).
[19] M. N. Gastiasoro, P. J. Hirschfeld, and B. M. Andersen, Impurity states and cooperative magnetic order in Fe-based superconductors, Phys. Rev. B **88**, 220509(R) (2013).
[20] T. Hanaguri, K. Kitagawa, K. Matsubayashi, Y. Mazaki, Y. Uwatoko, and H. Takagi, Scanning tunneling microscopy/spectroscopy of vortices in LiFeAs, Phys. Rev. B **85**, 214505 (2012); B. M. Uranga, M. N. Gastiasoro, and B. M. Andersen, Electronic vortex structure of Fe-based superconductors: Application to LiFeAs, Phys. Rev. B **93**, 224503 (2016).
[21] S. S. Zhang *et al.*, Vector field controlled vortex lattice symmetry in LiFeAs using scanning tunneling microscopy, Phys. Rev. B **99**, 161103(R) (2019).
[22] L. Fu and C. L. Kane, Superconducting Proximity Effect and Majorana Fermions at the Surface of a Topological Insulator, Phys. Rev. Lett. **100**, 096407 (2008).
[23] E. J. König and P. Coleman, Crystalline-Symmetry-Protected Helical Majorana Modes in the Iron Pnictides, Phys. Rev. Lett. **122**, 207001 (2019).
[24] S. Qin, L. Hu, C. Le, J. Zeng, F.-c. Zhang, C. Fang, and J. Hu, Quasi-1D Topological Nodal Vortex Line Phase in Doped Superconducting 3D Dirac Semimetals, Phys. Rev. Lett. **123**, 027003 (2019).
[25] See Supplemental Material at http://link.aps.org/supplemental/10.1103/PhysRevLett.123.217004 for calculation details, which includes Refs. [26–44].
[26] Q. Deng, X. Ding, S. Li, J. Tao, H. Yang, and H.-H. Wen, The effect of impurity and the suppression of superconductivity in $Na(Fe_{0.97-x}Co_{0.03}T_x)As$ (T = Cu, Mn), New J. Phys. **16**, 063020 (2014).
[27] P. Hohenberg and W. Kohn, Inhomogeneous electron gas, Phys. Rev. **136**, B864 (1964).
[28] W. Kohn and L. J. Sham, Self-consistent equations including exchange and correlation effects, Phys. Rev. **140**, A1133 (1965).
[29] G. Kresse and J. Hafner, Ab initio molecular dynamics for liquid metals, Phys. Rev. B **47**, 558 (1993).
[30] G. Kresse and J. Furthmüller, Efficient iterative schemes for ab initio total-energy calculations using plane-wave basis set, Phys. Rev. B **54**, 11169 (1996).
[31] J. P. Perdew, K. Burke, and M. Ernzerhof, Generalized Gradient Approximation made Simple, Phys. Rev. Lett. **77**, 3865 (1996).
[32] G. Kresse and D. Joubert, From ultrasoft pseudopotentials to the projector augmented-wave method, Phys. Rev. B **59**, 1758 (1999).
[33] H. J. Monkhorst and J. D. Pack, Special points for Brillouin-zone integrations, Phys. Rev. B **13**, 5188 (1976).
[34] K. Nakamura, R. Arita, and H. Ikeda, First-principles calculation of transition-metal impurities in LaFeAsO, Phys. Rev. B **83**, 144512 (2011).
[35] P. J. Hirschfeld, P. Wölfle, and D. Einzel, Consequences of resonant impurity scattering in anisotropic superconductors: Thermal and spin relaxation properties, Phys. Rev. B **37**, 83 (1988).
[36] T. Zhou, Z. D. Wang, Y. Gao, and C. S. Ting, Electronic structure around a vortex core in iron-based superconductors: Numerical studies of a two-orbital model, Phys. Rev. B **84**, 174524 (2011).
[37] T. Zhou, H. Huang, Y. Gao, J.-X. Zhu, and C. S. Ting, Quasiparticle states around a nonmagnetic impurity in electron-doped iron-based superconductors with spin-density-wave order, Phys. Rev. B **83**, 214502 (2011).
[38] Y. Y. Zhao, B. Li, W. Li, H.-Y. Chen, K. E. Bassler, and C. S. Ting, Effects of single- and multi-substituted Zn ions in doped 122-type iron-based superconductors, Phys. Rev. B **93**, 144510 (2016).
[39] Y. Gao, Y. Wang, T. Zhou, H. Huang, and Q.-H. Wang, Possible Pairing Symmetry in the FeSe-Based

Superconductors Determined by Quasiparticle Interference, Phys. Rev. Lett. **121**, 267005 (2018).

[40] Y. Wang, A. Kreisel, V. B. Zabolotnyy, S. V. Borisenko, B. Büchner, T. A. Maier, P. J. Hirschfeld, and D. J. Scalapino, Superconducting gap in LiFeAs from three-dimensional spin-fluctuation pairing calculations, Phys. Rev. B **88**, 174516 (2013).

[41] H. Eschrig and K. Koepernik, Tight-binding models for the iron-based superconductors, Phys. Rev. B **80**, 104503 (2009).

[42] A. Kreisel, B. M. Andersen, P. O. Sprau, A. Kostin, J. C. Séamus Davis, and P. J. Hirschfeld, Orbital selective pairing and gap structures of iron-based superconductors, Phys. Rev. B **95**, 174504 (2017).

[43] S. Kobayashi and M. Sato, Topological Superconductivity in Dirac Semimetals, Phys. Rev. Lett. **115**, 187001 (2015).

[44] T. Hashimoto, S. Kobayashi, Y. Tanaka, and M. Sato, Superconductivity in doped Dirac semimetals, Phys. Rev. B **94**, 014510 (2016).

[45] Y. Bang, H. Y. Choi, and H. Won, Impurity effects on the $\pm$s-wave state of the iron-based superconductors, Phys. Rev. B **79**, 054529 (2009).

[46] S. Onari and H. Kontani, Violation of Anderson's Theorem for the Sign-Reversing s-Wave State of Iron-Pnictide Superconductors, Phys. Rev. Lett. **103**, 177001 (2009).

[47] D. Zhang, Nonmagnetic Impurity Resonances as a Signature of Sign-Reversal Pairing in FeAs-Based Superconductors, Phys. Rev. Lett. **103**, 186402 (2009).

[48] A. Kreisel *et al.*, Towards a quantitative description of tunneling conductance of superconductors: Application to LiFeAs, Phys. Rev. B **94**, 224518 (2016).

[49] J.-X. Yin *et al.*, Giant and anisotropic many-body spin–orbit tunability in a strongly correlated kagome magnet, Nature (London) **562**, 91 (2018).